# Increase in CO₂ reduction rate via optical near-field effect

**Takashi Yatsui⬤,ᵃ,*,† Yuki Nakamura,ᵃ Yosuke Suzuki,ᵃ
Tatsuki Morimoto⬤,ᵇ Yuma Kato,ᶜ Muneaki Yamamoto,ᶜ
Tomoko Yoshida,ᶜ Wataru Kurashige,ᵈ Nobuyuki Shimizu,ᵈ
Yuichi Negishi⬤,ᵈ Kenji Iida⬤,ᵉ‡ and Katsuyuki Nobusadaᵉ**

ᵃUniversity of Tokyo, School of Engineering, Japan
ᵇTokyo University of Technology, School of Engineering, Hachioji, Japan
ᶜOsaka City University, Advanced Research Institute for Natural Science, Osaka, Japan
ᵈTokyo University of Science, Faculty of Science, Japan
ᵉInstitute for Molecular Science, Department of Theoretical and Computational Molecular
Science, Okazaki, Japan

**Abstract.** To reduce the effects of global warming, visible and near-infrared light must be used more efficiently. Deep ultraviolet light (8 eV) is required for the direct dissociation of $CO_2$ by light; however, the introduction of a metal complex has made it possible to realize $CO_2$ reduction with visible light. We demonstrate that the optical near field (ONF) can increase the $CO_2$ reduction rate. For this, we used gold clusters, because they can be a suitable source for ONFs, as their size and density can be controlled by the number of gold atoms. By attaching a metal complex near gold clusters with diameters of 1.0 to 1.3 nm, we confirm that the reduction rate of $CO_2$ to CO increased by 1.5 to 2.1 times. The gold clusters were sufficiently small; therefore, there was no plasmonic resonant peak or heat generation. Because the near-field effect is based on a photochemical reaction, it can be applied to other metal complexes used in $CO_2$ reduction, and it has other applications such as water splitting and water purification. © *The Authors. Published by SPIE under a Creative Commons Attribution 4.0 Unported License. Distribution or reproduction of this work in whole or in part requires full attribution of the original publication, including its DOI.* [DOI: 10.1117/1 .JNP.14.046011]

## 1 Introduction

The use of a metal complex for $CO_2$ reduction has increasingly attracted research attention. This is because of its ability to facilitate the use of visible light for $CO_2$ reduction,[1,2] which otherwise requires deep ultraviolet radiations to perform the direct dissociation of $CO_2$ owing to its large dissociation energy (∼8 eV).[3] Several metal complexes have been developed to realize the above objective, including Re,[4] Ru,[5] and Cu.[6–9] However, previous investigations on this topic mainly focused on the band engineering of materials using complexes. In a previous study, we developed a method to utilize the optical near field (ONF) generated near nanoscale materials.[10] ONF is applicable to all nanoscale materials irrespective of their type. However, field enhancement requires plasmon resonance; thus, its effects are only observed near the resonant wavelength of the metal complex. In addition, unique ONF properties, owing to which ONFs do not require plasmon resonance, have been investigated.[11–13] As the ONF is localized in the nanoscale range, it has a nonuniform optical field. This implies that the field gradient $\frac{\partial E}{\partial r}$ is nonzero near the nanoscale materials. For such a system, we found that ONFs inherently achieve strong second harmonic generation because they break the selection rule of this generation.[14,15] Furthermore,

---

ONFs can excite the dipole forbidden transition of various molecules.[10,16] These properties make it possible to utilize lower photon energies, which results in improved $CO_2$ reduction efficiency. Previously, we had demonstrated a redshift in the absorption spectra, following the introduction of a near-field source.[17] Therein, a Re-complex was attached to ZnO nanocrystalline aggregates with nanoprotrusions, which behaved as the near-field source. Note that the ZnO nanocrystal is a nonmetallic compound; therefore, the redshift observed in the absorption of $CO_2$ after the introduction of the near-field source of ZnO nanocrystal did not originate from the plasmon resonance. Because the redshift of the absorption of $CO_2$ improves the $CO_2$ reduction rate due to the usage of a longer wavelength than the absorption edge wavelength, ONFs are expected to improve the $CO_2$ reduction performance without plasmon resonance. However, the size and density distributions of the nanoprotrusions of the ZnO nanocrystalline aggregates were highly random. Therefore, it was difficult to determine the effect of the nanoprotrusions, definitively. The gold clusters can be used as a suitable ONF source, because their size and density can be controlled by the number of gold atoms.[18] In this work, we controlled the size and density of the near-field source by introducing gold clusters. The introduction of gold clusters was realized in a subnanometer-sized near-field source, which could observe the ONF effect without discrete electric structures and the plasmon effect. The enhanced absorption, attributed to the gold clusters, was used to improve the $CO_2$ reduction efficiency of the photoexcited carriers in the Re-complex.

## 2 Results

### 2.1 Au Cluster Attachment

To control the size of ONF sources, we used gold clusters. To arrange the gold clusters in the vicinity of the metal complex, first, the gold clusters were deposited on an alumina sphere, and then the metal complex was deposited on the alumina sphere (see Sec. 2.2). We used the alumina sphere [AO-502 (Admatechs)] with a median particle diameter in the range 200 to 300 nm. Glutathione-protected $Au_{25}$ $[Au_{25}(SG)_{18}]$ was used as the precursor for the gold clusters.[18] This $Au_{25}$ was attached to the alumina sphere after stirring in water in a manner similar to that described in previous studies.[18–20] In particular, $Au_{25}(SG)_{18}$ clusters were adsorbed on the alumina sphere by mixing an aqueous solution containing $Au_{25}(SG)_{18}$ with an aqueous solution of alumina sphere (600 mg) for 2 h at room temperature (~20℃). The total volume of the aqueous solution was fixed at 200 mL, and the mixing ratio of the $Au_{25}(SG)_{18}$ clusters to the alumina sphere was fixed at 0.05, 0.1, or 0.2 wt. % Au. Because glutathione was simply used as a linker between alumina and gold clusters, it was eliminated by firing at 300℃ for 2 h. Here, we expected to observe the ONF effect without the discrete electric structures and plasmon effect. We selected $Au_{25}$ because the number of gold atoms is sufficiently small to ensure there is no plasmonic resonant peak, which is observed when the number of Au atoms exceeds 144.[21] In addition, the attached clusters were fired so that the discrete electric structures disappeared.[21]

To confirm the attachment of gold clusters on the alumina sphere, we compared the absorbance of gold clusters between before and after attachment on the alumina sphere [Fig. 1(a)]. A comparison of the UV-visible spectra of gold clusters [black solid curve in Fig. 1(a) taken before attachment] with the diffuse reflectance (DR) spectra of gold clusters taken after attachment on alumina sphere [before firing, blue solid curve in Fig. 1(a)] showed that the discrete peaks disappeared after firing in the DR spectra [red solid curve in Fig. 1(a)]. This indicates that the atomicity was destroyed after firing.

We also conducted inductively coupled plasma mass spectrometry (ICP-MS) analysis.[19,22] Bi was used as an internal standard. The ICP-MS analysis of the solutions after stirring was conducted to estimate the quantity of Au that was not adsorbed onto the alumina sphere. We found that the gold clusters were almost adsorbed on the alumina sphere with an average adsorption efficiency of 92.1%. Glutathione molecules contain multiple polar carboxyl and amino functional groups. In addition, when metal oxide is added to water, hydroxyl groups (─OH) are normally formed on the surface. Therefore, it can be considered that $Au_{25}(SG)_{18}$ was efficiently adsorbed onto the alumina owing to the formation of hydrogen bonds between the ─OH groups on the surface of the alumina and the glutathione functional groups, as often observed in previous
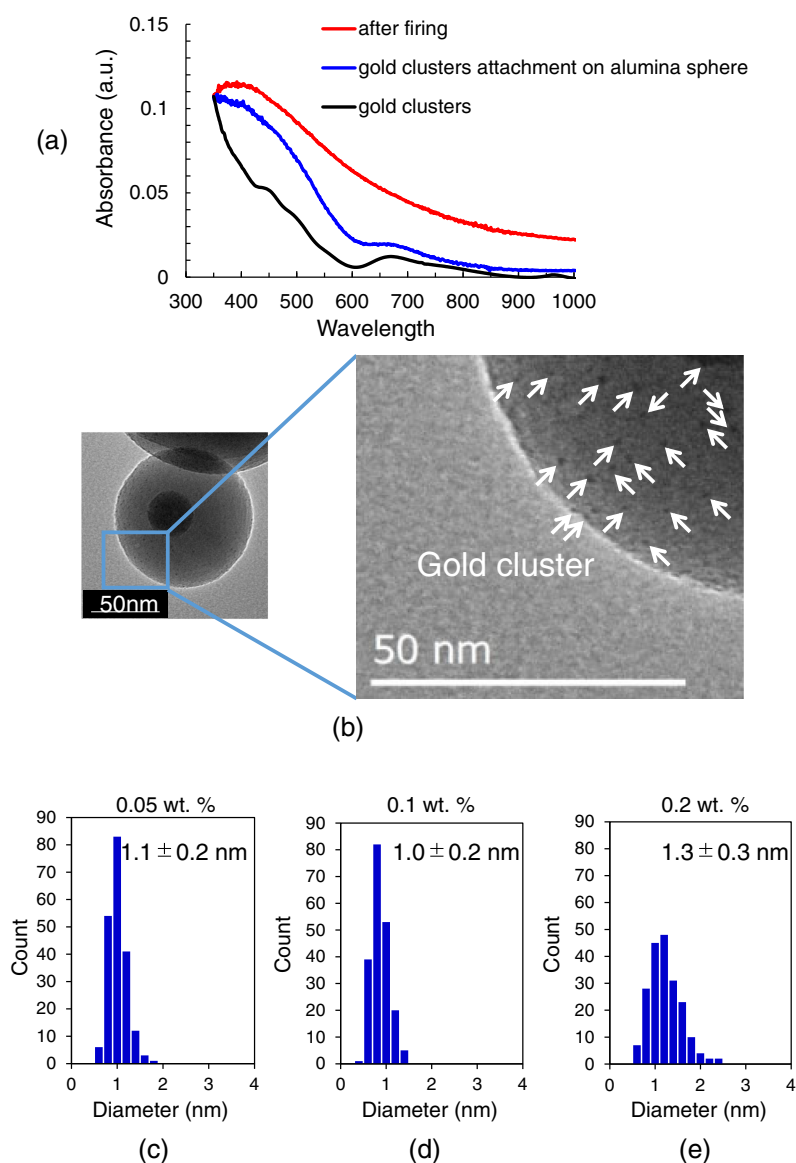
**Fig. 1** (a) Comparison of absorbance. Black (before attachment): UV-visible spectra of gold clusters $[Au_{25}(SG)_{18}]$ only, blue (after attachment): DR spectra of gold clusters attached on alumina sphere, and red (after attachment): DR spectra of gold clusters attached on alumina sphere after firing. (b) TEM image of the gold clusters on alumina sphere. Black dots indicated by white arrows are gold clusters. Size distribution of gold clusters with glutathione-protected $Au_{25}$ with density of (c) 0.05 wt. %, (d) 0.1 wt. %, and (e) 0.2 wt. %.

studies.[19,22] This high adsorption efficiency allowed us to obtain a high reproducibility of the adsorption of $Au_{25}(SG)_{18}$ on the surface of the alumina.

Figure 1(b) shows the typical transmission electron microscope (TEM) images of the gold clusters on an alumina sphere. The sizes of the gold clusters were evaluated from the TEM images. As shown in Figs. 1(c)–1(e), the sizes of the gold clusters were in the range 1.0 to 1.3 nm, with monodispersed size. The size range was below the threshold diameter of 1.6 nm for the plasmon peak.[21]

## 2.2 Re-Complex Attachment

We used $Re(bpy\text{-}COOH)(CO)_3Cl$ (bpy-COOH = 2,2′-bipyridine-4,4′-dicarboxylic acid), abbreviated as Re(bpy–COOH),[23] as an Re-complex (metal complex) to investigate the ONF

effect on $CO_2$ reduction. As described in Ref. 24, first, $Re(CO)_5Cl$ was dissolved in methanol. An equimolar amount of 2,2′-bipyridine-4,4′-dicarboxylic acid was added to the solution, and the produced mixture was stirred under reflux, producing Re(bpy-COOH) [see Fig. 2(a)]. Second, to attach Re(bpy-COOH) to the alumina sphere with gold clusters, Re(bpy-COOH) was dissolved in acetonitrile. Then, the Re(bpy-COOH) solution was mixed with the alumina-containing solution, and the mixture was allowed to stand still for 8 h in a manner similar to that of a previous study.[17] Through this process, Re(bpy-COOH) could attach to the alumina surface because of the deprotonation of the carboxyl group.

To confirm the attachment of Re(bpy-COOH) on the alumina sphere, we obtained the Fourier transform infrared (FTIR) spectra using the KBr tablet method by Shimadzu IRPrestige-21 [see Figs. 2(b) and 2(c)]. In all measurements, we used 0.02 g of the samples. We focused on the wavenumber range corresponding to the carbonyl vibrational stretching modes: an out-of-phase symmetric mode; an asymmetric mode, primarily, among the two equatorial carbonyls; and an in-phase symmetric mode.[25] As shown in Fig. 2(b), the curve of Re(bpy-COOH) has three peaks at $\sim$2034, 1930, and 1880 $cm^{-1}$, corresponding to the carbonyl vibrational stretching modes, respectively. Figure 2(c) shows the FTIR spectra of the Re(bpy-COOH) attached to the alumina sphere with different gold densities. Because the amount of Re-complex attached to the alumina sphere was small, the absorbance was considerably smaller than that of Re-complex only, shown in Fig. 2(b). Therefore, the lower two peaks at considerably 1930 and 1880 $cm^{-1}$ were degenerated, and the curves had a broad peak around 1920 $cm^{-1}$, in addition to the peak at $\sim$2030 $cm^{-1}$. From these results, it is confirmed that the Re-complex was attached to the aluminum sphere.
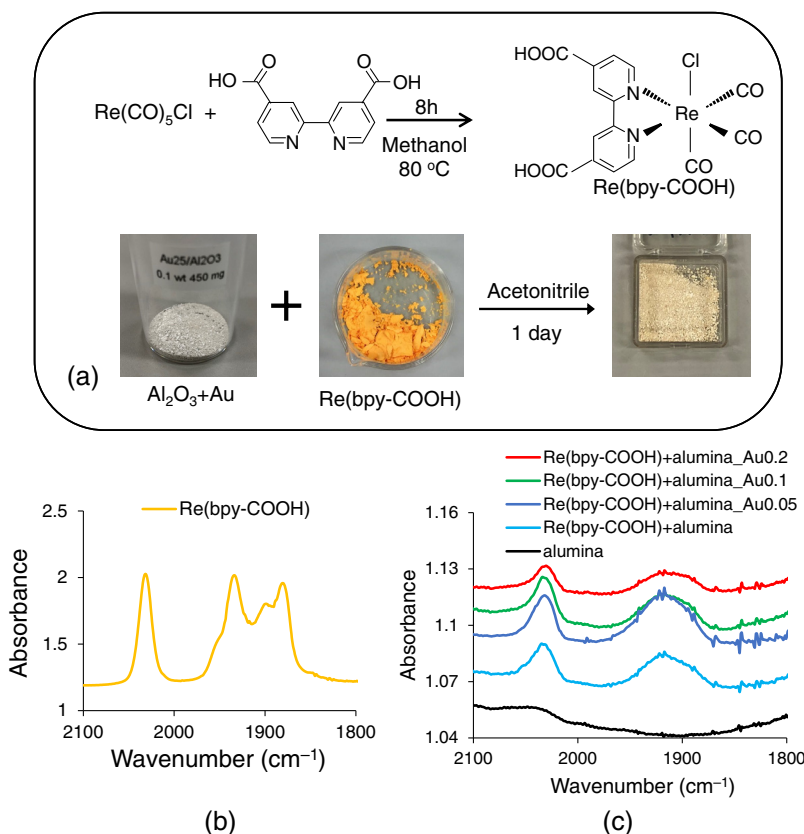


**Fig. 2** (a) Schematic of the Re-complex attachment onto alumina sphere with gold clusters. FTIR spectra of (b) Re(bpy-COOH) and (c) Re(bpy-COOH) with alumina sphere. Black (alumina): alumina sphere only, blue [Re(bpy-COOH)+alumina]: Re(bpy-COOH) with alumina sphere, purple [Re(bpy-COOH)+alumina_Au0.05]: Re(bpy-COOH) with alumina sphere with gold density of 0.05 wt. %, green [Re(bpy-COOH)+alumina_Au0.1]: Re(bpy-COOH) with alumina sphere with gold density of 0.1 wt. %, and red [Re(bpy-COOH)+alumina_Au0.2]: Re(bpy-COOH) with alumina sphere with gold density of 0.2 wt. %.

## 2.3 *Evaluation of the Absorption Spectra Change Following the Gold-Cluster Attachment*

To check the effects of gold-cluster attachment in the vicinity of the Re-complex, we obtained the diffuse reflection spectra corresponding to the absorption spectra, using a spectrophotometer (JASCO V-670). Figure 3(a) shows the Kubelka–Munk plots of the diffuse reflection spectra[26] of Re(bpy-COOH) (solid black curve) and Re(bpy-COOH) attached to the alumina sphere with different gold-cluster densities. Two main peaks were observed at ∼310 (peak 1) and 410 (peak 2) nm, corresponding to the $\pi - \pi*$ transition and metal-to-ligand charge transfer (MLCT) transition, respectively.[27] Figure 3(b) shows the $Au_{25}$ density and peak wavelength dependence of the absorption peak. The peak value of peak 1 decreased following the attachment of gold clusters. The peak value of peak 2 increased as the $Au_{25}$ density increased, which could be caused by the field-enhancement effect of the ONF.[17] As described in our previous paper,[17] if the direction of the incident light polarization is the same as that of the dipole field induced by the electronic polarization of nanoparticles, the dipole field enhances the electric field acting on the Re-complex and increases its absorption intensity [Fig. 3(c)]. This assumption was numerically supported by the first-principle calculations. We expect the density of gold clusters to increase as the $Au_{25}$ density increased, it is reasonable that the peak value of peak 2 increased as the $Au_{25}$ density increased. Based on our previous studies,[17] we consider that the field enhancement can be dominant contributor to the increase in the CO₂ reduction rate. However, the contribution of ONF depends on the geometrical arrangement of the Re-complex and the details of the geometrical and electric structures of the gold clusters. The main purpose of this study was to enhance the CO₂ reduction rate using subnanometer gold without plasmon resonance. Note that the spectrum of Re(bpy-COOH) on an alumina sphere with a gold density of 0.2 wt. % [red solid curve
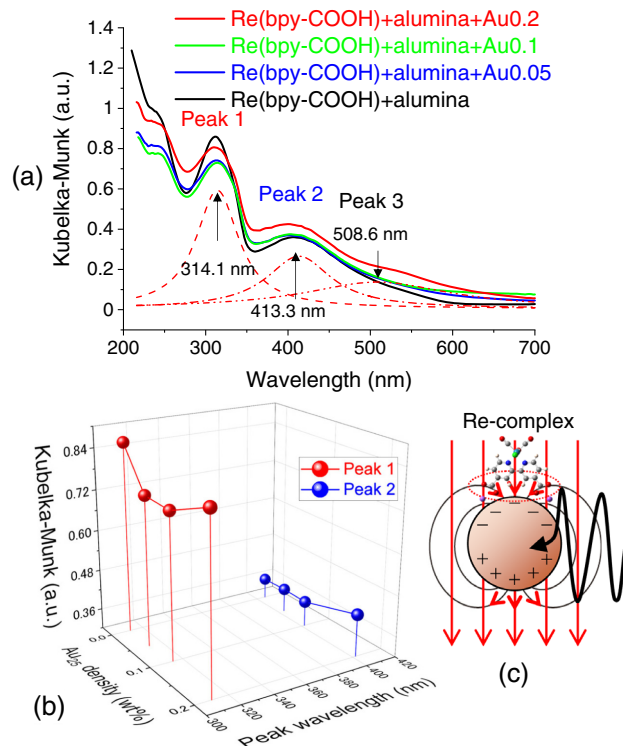


**Fig. 3** (a) Diffuse reflection spectra. Black solid curve: Re(bpy-COOH) deposited on alumina sphere, blue solid curve: Re(bpy-COOH) and gold cluster (with density 0.05 wt. %) deposited on alumina sphere, green solid curve: Re(bpy-COOH) and gold cluster (with density 0.1 wt. %) deposited on alumina sphere, and red solid curve: Re(bpy-COOH) and gold cluster (with density 0.2 wt. %) deposited on alumina sphere. (b) $Au_{25}$ density and peak wavelength dependence of the absorption peaks. (c) Field enhancement as shown in the dashed red circles owing to the electronic polarization of nanostructure.[17]

in Fig. 3(a)] has an additional peak (peak 3) at ~510 nm. To evaluate the change further, we fitted the curve using three Lorentzian peaks at ~314.1 (peak 1), 413.3 (peak 2), and 508.6 nm (peak 3). The peak wavelength of peak 3 was similar to the plasmon peak of the gold clusters.[28] However, the plasmon peak in the absorption spectra of the gold clusters could be observed only when the diameter exceeded 1.6 nm.[21] In addition, we observed a similar peak at ~510 nm when using ZnO nanocrystalline aggregates, i.e., no gold.[17] Therefore, peak 3 might not have been caused by the plasmon resonance. Several reports have been published on the thermal effects in metallic nanoparticles.[29,30] The temperature increase can be described as follows:[31]

$$\Delta T = \frac{I_{inc} C_{sca}}{4\pi k a}, \tag{1}$$

where $I_{inc}$ is the incident light intensity (~50 mW/cm²), $a$ is the diameter of the gold cluster (~0.5 nm), $C_{sca}$ is the absorption cross-section of the gold cluster $\left(= 4\pi\left(\frac{2\pi}{\lambda}\right)a^3 \text{Im}\left[\frac{\varepsilon-1}{\varepsilon+2}\right]\right) = 1.1 \times 10^{-16}$ cm² for $\lambda = 405$ nm, $a = 0.5$ nm, and $\varepsilon = -1.7 + i\,6.5$),[28,32] and $k$ is the thermal conductivity of the alumina sphere (~0.7 W/m · K).[33] Thus, the value of $\Delta T$ can be estimated to be on the order of nK. Therefore, it is expected that the thermal effect can be eliminated completely.

## 2.4 CO₂-Reduction Experiment

As the gold-cluster attachment enhanced the absorbance, we performed a CO₂ reduction experiment [Fig. 4(a)]. CO₂ gas was dissolved in dimethylformamide (DMF)/triethanolamine (TEOA) mixed solution (DMF/TEOA = 1 mL/0.2 mL).[34] A laser light of wavelength 405 nm (50 mW) was used for the CO₂ reduction experiment because this wavelength was closed to peak 2 and the
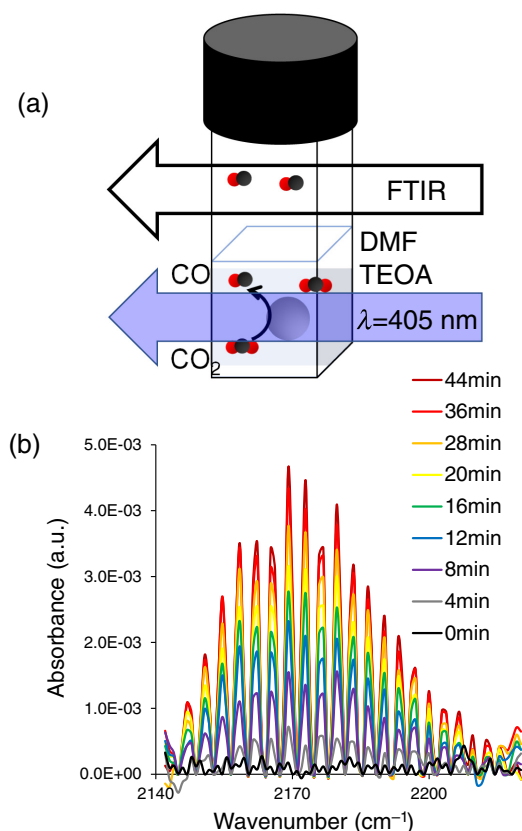


**Fig. 4** (a) Schematic of CO₂ reduction experiment. (b) Time dependence of the normalized CO absorption spectra.

difference of Kubelka–Munk intensities between 405 and 413.3 nm were ~1%, where the absorbance increased because of the gold-cluster attachment owing to the field-enhancement effect of the ONF[17] [see Fig. 3(a)]. In all experiments, we used 30 mg of Re-complex with the alumina sphere. We detected the CO generation using the FTIR spectra from Shimadzu IRPrestige-21. Because the CO spectra showed strong absorption in the synthetic silica below 2100 cm$^{-1}$, we used a cell of anhydrous synthetic quartz (S15-IR-10, GL Sciences). Figure 4(b) shows the normalized absorption spectra of the R branch of Re(bpy-COOH) on an alumina sphere with the gold density of 0.2 wt. %, which was normalized with respect to that of the cell.[35] Note that these spectra were not obtained using the cell of synthetic silica.

To evaluate the CO$_2$ reduction rate, we plotted the absorbance at the spectral peaks. Figure 5 shows the Au$_{25}$ density dependence. In all plots, the absorbance was found to be saturated. The saturation could be attributed to the degradation of Re(bpy-COOH). Because Re(bpy-COOH)(CO)$_3$Cl has three CO as ligands, Re(bpy-COOH) causes both the degradation of Re(bpy-COOH)(CO)$_3$Cl and CO$_2$ reduction.[36] Regardless of the degradation of Re(bpy-COOH), it was found that the CO generation rate increased following the gold-cluster attachment, compared with the rate without the gold clusters. To evaluate this increase, we fitted the data as[36]

$$[CO_{red}]_t = [CO_{red}]_{t=\infty} \times \{1 - \exp(-k_{red}t)\}, \tag{2}$$

where CO$_{red}$ is the CO produced by CO$_2$ reduction, $[CO_{red}]_t$ is the absorbance of the CO produced by CO$_2$ reduction at time $t$, $[CO_{red}]_{t=\infty}$ is the total amount of CO$_{red}$ produced, and $k_{red}$ is the CO$_2$ reduction rate. The amount of Re-complex depends on the amount of gold clusters and the aluminum sphere size. Therefore, the absolute values of the CO absorption peaks should depend on the experiment. However, the absorption value should saturate when all Re-complex degrade. Thus, the absorbance was normalized by $[CO_{red}]_{t=\infty}$, which depends on the amount of Re-complex. Table 1 compares the increased $k_{red}$ with the rate obtained without the gold clusters. From the results, it was confirmed that the rate of reduction to CO increased by 1.5 to 2.1 times upon introducing the gold clusters. This increase was greater than the increase in the absorbance at the wavelength of peak 2 (MLCT transition peak), by a factor of 1.2 (maximum increased value for gold cluster density of 0.2 wt. % in comparison with that without a gold cluster), as shown in Fig. 3(a). As previously reported, the MLCT transition peak of the Re-complex was enhanced following the introduction of a nanostructure because of the field-enhancement effect of the ONF.[17] As reported in a previous study,[17] the absorption intensity increased by a factor of 2.0, which was comparable to the observed value of the increased rate of reduction to CO.
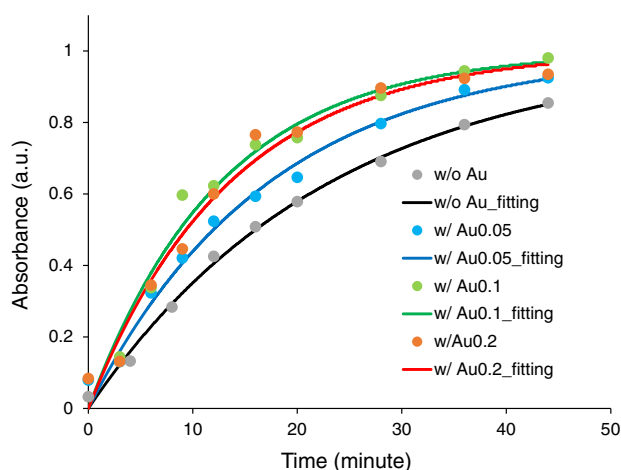


**Fig. 5** Normalized time-dependent absorption peak at 2169 cm$^{-1}$ for different Au$_{25}$ densities. w/o Au: Re(bpy-COOH) with alumina sphere without gold clusters, w/ Au0.05: Re(bpy-COOH) with alumina sphere with Au$_{25}$ density of 0.05 wt. %, w/ Au0.1: Re(bpy-COOH) with alumina sphere with Au$_{25}$ density of 0.1 wt. %, and w/ Au0.2: Re(bpy-COOH) with alumina sphere with Au$_{25}$ density of 0.2 wt. %.

**Table 1** Increased rates of in the $CO_2$ reduction rate $k_{red}$.

| Au$_{25}$ density | Wavenumber (cm$^{-1}$) | | | |
| --- | --- | --- | --- | --- |
| | 2165 | 2169 | 2173 | 2177 |
| 0.05 wt. % | 1.58 | 1.34 | 1.53 | 1.39 |
| 0.1 wt. % | 1.62 | 1.83 | 1.93 | 1.72 |
| 0.2 wt. % | 1.34 | 1.71 | 1.52 | 2.09 |

The $CO_2$ reduction rate increased with the introduction of gold clusters. However, the $CO_2$ reduction rate of 0.1 wt. % was the maximum value (in comparison with 0.05 and 0.2 wt. %) in most of absorption peaks except the peak at 2177 cm$^{-1}$ (see Table 1). In the current experiment, the distance between the gold clusters and Re was random, and the position of Re was not controlled. More detailed investigation can be performed using the thiol-gold interaction by introducing thiol in the Re-complex.

## 3 Conclusions

We demonstrated that Re-complexes with size-controlled nanostructures of gold clusters had stronger absorptions, compared with that without nanostructures. This phenomenon was applied to $CO_2$ reduction. The results indicated that the enhancement of the MLCT excitation of the Re-complex increased the reduction rate of $CO_2$ to CO by a factor of 1.5 to 2.1. Because the proposed system utilized gold clusters, the introduction of thiol into the metal complex, resulting in gold–thiol coupling, will result in the higher controllability of the separation and positioning of the gold and metal complex. Further, higher $CO_2$ reduction rates can be achieved. This observed effect could be applied to $CO_2$ reduction using metal-complex materials—not only the Re-complex but also other metal complexes including Ru[37] and Cu.[6]

## Acknowledgments

## References

1. H. Takeda et al., "Development of an efficient photocatalytic system for $CO_2$ reduction using rhenium(i) complexes based on mechanistic studies," *J. Am. Chem. Soc.* **130**, 2023–2031 (2008).
2. R. Kuriki et al., "Visible-light-driven $CO_2$ reduction with carbon nitride: enhancing the activity of ruthenium catalysts," *Angew. Chem. Int. Ed.* **54**, 2406–2409 (2015).
3. Z. Chen et al., "Imaging $CO_2$ photodissociation at 157 nm: state-to-state correlations between $CO(\nu)$ and $O(^3P_{j=0,1,2})$," *J. Phys. Chem. Lett.* **1**, 1861–1865 (2010).
4. J. Hawecker, J.-M. Lehn, and R. Ziessel, "Photochemical and electrochemical reduction of carbon dioxide to carbon monoxide mediated by (2,2′-bipyridine)tricarbonylchlororhenium(I) and related complexes as homogeneous catalysts," *Helv. Chim. Acta* **69**, 1990–2012 (1986).
5. C. A. Craig et al., "Photochemical reduction of carbon dioxide using nickel tetraazamacrocycles," *J. Phys. Chem.* **94**, 7957–7960 (1990).
6. H. Takeda et al., "Development of visible-light driven Cu(I) complex photosensitizers for photocatalytic $CO_2$ reduction," *Front. Chem.* **7**, 418 (2019).

7. L. Wang et al., "Anchored Cu(II) tetra(4-carboxylphenyl)porphyrin to P25 (TiO$_2$) for efficient photocatalytic ability in CO$_2$ reduction," *Appl. Catal., B* **239**, 599–608 (2018).

8. L. Wang et al., "*In-situ* incorporation of copper(II) porphyrin functionalized zirconium MOF and TiO$_2$ for efficient photocatalytic CO$_2$ reduction," *Sci. Bull.* **64**, 926–933 (2019).

9. L. Wang et al., "Integration of copper(II)-porphyrin zirconium metal–organic framework and titanium dioxide to construct Z-scheme system for highly improved photocatalytic CO$_2$ reduction," *ACS Sustainable Chem. Eng.* **7**, 15660–15670 (2019).

10. T. Yatsui, M. Yamaguchi, and K. Nobusada, "Nano-scale chemical reactions based on non-uniform optical near-fields and their applications," *Prog. Quantum Electron.* **55**, 166–194 (2017).

11. A. J. Welch et al., "Nanoporous gold as a highly selective and active carbon dioxide reduction catalyst," *ACS Appl. Energy Mater.* **2**, 164–170 (2019).

12. P. Novello, C. V. Varanasi, and J. Liu, "Effects of light on catalytic activities and lifetime of plasmonic Au catalysts in the CO oxidation reaction," *ACS Catal.* **9**, 578–586 (2019).

13. S. Tan et al., "Plasmonic coupling at a metal/semiconductor interface," *Nat. Photonics* **11**, 806–812 (2017).

14. M. Yamaguchi et al., "Two-photon absorption induced by electric field gradient of optical near-field and its application to photolithography," *Appl. Phys. Lett.* **106**, 191103 (2015).

15. M. Yamaguchi, K. Nobusada, and T. Yatsui, "Nonlinear optical response induced by a second-harmonic electric-field component concomitant with optical near-field excitation," *Phys. Rev. A* **92**, 043809 (2015).

16. M. Yamaguchi and K. Nobusada, "Photodissociation path in H$^{2+}$ induced by nonuniform optical near fields: two-step excitation via vibrationally excited states," *Phys. Rev. A* **93**, 023416 (2016).

17. T. Yatsui et al., "Realization of red shift of absorption spectra using optical near-field effect," *Nanotechnology* **30**, 34LT02 (2019).

18. Y. Negishi et al., "Enhanced photocatalytic water splitting by BaLa$_4$Ti$_4$O$_{15}$ loaded with ∼1 nm gold nanoclusters using glutathione-protected Au$_{25}$ clusters," *Nanoscale* **5**, 7188–7192 (2013).

19. Y. Negishi et al., "Controlled loading of small Au$_n$ clusters ($n = 10$–39) onto BaLa$_4$Ti$_4$O$_{15}$ photocatalysts: toward an understanding of size effect of cocatalyst on water-splitting photocatalytic activity," *J. Phys. Chem. C* **119**, 11224–11232 (2015).

20. T. Kawawaki et al., "Controlled colloidal metal nanoparticles and nanoclusters: recent applications as cocatalysts for improving photocatalytic water-splitting activity," *J. Mater. Chem. A* **8**, 16081–16113 (2020).

21. Y. Negishi et al., "A critical size for emergence of nonbulk electronic and geometric structures in dodecanethiolate-protected Au clusters," *J. Am. Chem. Soc.* **137**, 1206–1212 (2015).

22. W. Kurashige et al., "Atomic-level understanding of the effect of heteroatom doping of the cocatalyst on water-splitting activity in AuPd or AuPt alloy cluster-loaded BaLa$_4$Ti$_4$O$_{15}$," *ACS Appl. Energy Mater.* **2**, 4175–4187 (2019).

23. Y. Ono et al., "Effect of substituent groups in rhenium bipyridine complexes on photocatalytic CO$_2$ reduction," *Am. J. Appl. Chem.* **2**, 74–79 (2014).

24. J. M. Smieja and C. P. Kubiak, "Re(bipy-tBu)(CO)$_3$Cl–improved catalytic activity for reduction of carbon dioxide: IR-spectroelectrochemical and mechanistic studies," *Inorg. Chem.* **49**, 9283–9289 (2010).

25. L. M. Kiefer and K. J. Kubarych, "Solvent-dependent dynamics of a series of rhenium photoactivated catalysts measured with ultrafast 2DIR," *J. Phys. Chem. A* **119**, 959–965 (2015).

26. P. Kubelka, "New contributions to the optics of intensely light-scattering materials. Part I," *J. Opt. Soc. Am.* **38**, 448–457 (1948).

27. D. A. Kurtz et al., "Bathochromic shifts in rhenium carbonyl dyes induced through destabilization of occupied orbitals," *Inorg. Chem.* **57**, 5389–5399 (2018).

28. C. F. Bohren and D. R. Huffman, *Absorption and Scattering of Light by Small Particles*, Wiley, Weinheim, Germany (1998).

29. L. Zhou et al., "Quantifying hot carrier and thermal contributions in plasmonic photocatalysis," *Science* **362**, 69–72 (2018).

30. Y. Dubi, I. W. Un, and Y. Sivan, "Thermal effects—an alternative mechanism for plasmon-assisted photocatalysis," *Chem. Sci.* **11**, 5017–5027 (2020).
31. I. W. Un and Y. Sivan, "Parametric study of temperature distribution in plasmon-assisted photocatalysis," *Nanoscale* **12**, 17821–17832 (2020).
32. E. D. Palik, *Handbook of Optical Constants of Solids*, Academic, Massachusetts (1985).
33. H. Xie et al., "Thermal conductivity enhancement of suspensions containing nanosized alumina particles," *J. Appl. Phys.* **91**, 4568–4572 (2002).
34. T. Morimoto et al., "$CO_2$ capture by a rhenium(I) complex with the aid of triethanolamine," *J. Am. Chem. Soc.* **135**, 16825–16828 (2013).
35. D. C. Harris and M. D. Bertolucci, *Symmetry and Spectroscopy*, Dover Publications, New York (1989).
36. Y. Ono et al., "Kinetic study on $CO_2$ photoreduction by Re complexes," *J. Phys. Conf. Ser.* **379**, 012037 (2012).
37. R. Kuriki et al., "Robust binding between carbon nitride nanosheets and a binuclear Ruthenium(II) complex enabling durable, selective $CO_2$ reduction under visible light in aqueous solution," *Angew. Chem.* **129**, 4945–4949 (2017).

Biographies of the authors are not available.